Speed-dependent chemotactic precision in marine bacteria

Kwangmin Son[a,b,1], Filippo Menolascina[c,d], and Roman Stocker[b,e,1]

[a]Department of Mechanical Engineering, Massachusetts Institute of Technology, Cambridge, MA 02139; [b]Department of Civil and Environmental Engineering, Massachusetts Institute of Technology, Cambridge, MA 02139; [c]Institute for Bioengineering, The University of Edinburgh, Edinburgh EH9 3DW, United Kingdom; [d]Centre for Synthetic and Systems Biology, The University of Edinburgh, Edinburgh EH9 3BF, United Kingdom; and [e]Institute for Environmental Engineering, Department of Civil, Environmental and Geomatic Engineering, Eidgenössische Technische Hochschule (ETH) Zürich, 8093 Zurich, Switzerland

Edited by Victor Sourjik, Max Planck Institute for Terrestrial Microbiology, Marburg, Germany, and accepted by Editorial Board Member Herbert Levine June 10, 2016 (received for review February 10, 2016)

Chemotaxis underpins important ecological processes in marine bacteria, from the association with primary producers to the colonization of particles and hosts. Marine bacteria often swim with a single flagellum at high speeds, alternating "runs" with either 180° reversals or ∼90° "flicks," the latter resulting from a buckling instability of the flagellum. These adaptations diverge from *Escherichia coli*'s classic run-and-tumble motility, yet how they relate to the strong and rapid chemotaxis characteristic of marine bacteria has remained unknown. We investigated the relationship between swimming speed, run–reverse–flick motility, and high-performance chemotaxis by tracking thousands of *Vibrio alginolyticus* cells in microfluidic gradients. At odds with current chemotaxis models, we found that chemotactic precision—the strength of accumulation of cells at the peak of a gradient—is swimming-speed dependent in *V. alginolyticus*. Faster cells accumulate twofold more tightly by chemotaxis compared with slower cells, attaining an advantage in the exploitation of a resource additional to that of faster gradient climbing. Trajectory analysis and an agent-based mathematical model revealed that this unexpected advantage originates from a speed dependence of reorientation frequency and flicking, which were higher for faster cells, and was compounded by chemokinesis, an increase in speed with resource concentration. The absence of any one of these adaptations led to a 65–70% reduction in the population-level resource exposure. These findings indicate that, contrary to what occurs in *E. coli*, swimming speed can be a fundamental determinant of the gradient-seeking capabilities of marine bacteria, and suggest a new model of bacterial chemotaxis.

ocean | motility | run–reverse–flick | chemotaxis | chemokinesis

Motility is an essential component of chemotaxis (1), the ability of organisms to sense chemical gradients and swim toward more favorable conditions, for example, to find dissolved or particulate nutrients, colonize and infect hosts, or evade noxious substances (2). Most of our knowledge of bacterial chemotaxis comes from the study of *Escherichia coli*, a bacterium that inhabits the lower intestine of warm-blooded animals and swims using multiple (4–10) flagella (2). Counterclockwise (CCW) rotation of all motors causes the flagella to bundle and to propel the cell into a nearly straight "run" at 10–30 μm/s (2). A change in swimming direction occurs when one or more motors switch to clockwise (CW) rotation, disrupting the flagellar bundle and leading to a nearly random reorientation or "tumble" (2). The key to success in *E. coli*'s chemotaxis strategy is the bacterium's ability to control the switching frequency between CCW and CW flagellar rotation, giving rise to the well-known run-and-tumble swimming pattern (2). In this process, the swimming speed remains largely unchanged, and despite the bacterium's ability to sense mechanical stimuli (3), it is generally held that its chemotaxis depends only on the sensing of chemical stimuli. Consequently, the swimming speed has not been considered to affect the ability of cells to retain position in favorable regions of a gradient and does not enter into classic models of *E. coli*'s chemotaxis, beyond simply allowing proportionately faster climbing of a gradient (4).

Marine bacteria often exhibit higher chemotactic speed and precision than *E. coli*, showing faster gradient climbing and better steady-state accumulation at resource peaks (5, 6). These characteristics make marine bacteria a valuable model system to understand the limits of chemotaxis in microorganisms (7). For example, the marine bacterium *Pseudoalteromonas haloplanktis* was observed to respond up to 10-fold more rapidly than *E. coli* to resource pulses (5). The coastal marine bacterium *Vibrio alginolyticus* was found to accumulate threefold faster and sevenfold more tightly than *E. coli* toward serine (6). These high chemotactic performances are certainly caused at least in part by high swimming speeds, a common adaptation in marine bacteria (5, 8). However, a quantitative analysis has shown that simply rescaling *E. coli*'s speed to that of marine bacteria is not sufficient to explain the differences in their chemotactic performance (7), pointing at the need to better understand how the latter depends on the swimming pattern overall.

Analysis of a collection of ∼600 motile species of marine bacteria has shown that the majority (>90%) have a single, polar flagellum (9). The swimming patterns of marine bacteria have long been known to differ from *E. coli*'s run-and-tumble swimming (6, 10) by not displaying classic tumbles (8). However, only recently has a clearer picture emerged for the motility pattern of marine bacteria (6) and the underlying biomechanics (10), based on

Significance

Our understanding of bacterial chemotaxis, a fundamental nutrient-seeking strategy in the microbial world, mainly derives from *Escherichia coli*. However, it has become clear that marine bacteria evolved fundamentally different chemotaxis adaptations, often allowing them to accumulate at resource peaks more tightly and rapidly than *E. coli*. We studied the origin of this high chemotactic precision and found that it lies in an unexpected dependence of chemotaxis on swimming speed: faster cells have substantially higher precision, counter to all known models of chemotaxis. We elucidate this finding through a combination of single-cell tracking of thousands of marine bacteria in microfluidic gradients and a mathematical model of chemotaxis that explicitly accounts for swimming speed in the chemotaxis pathway.

Author contributions: K.S., F.M., and R.S. designed research; K.S. performed research; K.S. and F.M. contributed new reagents/analytic tools; K.S. analyzed data; and K.S., F.M., and R.S. wrote the paper.

The authors declare no conflict of interest.

This article is a PNAS Direct Submission. V.S. is a guest editor invited by the Editorial Board.

[1]To whom correspondence may be addressed. Email: kwangms@mit.edu or romanstocker@ethz.ch.

This article contains supporting information online at www.pnas.org/lookup/suppl/doi:10.1073/pnas.1602307113/-/DCSupplemental.

detailed observations of *V. alginolyticus*. *V. alginolyticus* alternates between forward and backward runs, and reorients by 180° reversals or 90° (on average) "flicks" (6). The flick arises from a large, off-axis deformation of the flagellum (6) caused by the buckling of the hook (10), a ∼100-nm-long, flexible structure that connects the flagellar filament to the rotary motor. The probability of a flick occurring during each run–reverse–flick cycle, P_F, is swimming-speed dependent, because the compressive load that causes buckling increases with speed (10), resulting in a sharp transition of the motility pattern from "run–reverse" to "run–reverse–flick" with increasing swimming speed (10). Thus, in contrast to *E. coli*, the motility pattern of *V. alginolyticus* is swimming-speed dependent. However, how this dependence on speed affects chemotactic performance has remained unknown.

A second important adaptation of several species of marine bacteria is chemokinesis (11, 12), the ability to modulate swimming speed in response to the concentration of a chemical (*SI Text*). The origin of chemokinesis remains largely unknown, and *E. coli* is generally believed to not display chemokinesis (13) [although some recent findings have questioned this model (14)]. Chemokinesis can enhance chemotaxis by increasing the speed of the cells, and thus the rate at which they climb chemical gradients (11), and also shifting the distribution of speeds within a population into a regime where flicks are predominant.

By focusing on these two speed-dependent motility adaptations in marine bacteria—flicking and chemokinesis—we study the chemotactic performance of *V. alginolyticus* as a function of the cells' swimming speed. In contrast to chemotaxis in *E. coli* and to current mathematical predictions, we find that the steady-state chemotactic accumulation of *V. alginolyticus* in a chemical gradient is speed dependent. A mathematical model of chemotaxis in marine bacteria that captures these observations suggests that swimming speed is an important parameter in their chemotaxis pathway, and helps explain the fast swimming speeds often observed among bacteria from the ocean.

Results

Dependence of Chemotaxis on Swimming Speed. A steady linear concentration profile ("linear gradient") of the amino acid serine, a chemoattractant for *V. alginolyticus* (6), was generated in a purposely engineered microfluidic device (Figs. S1 and S2, and *Materials and Methods*). The serine concentration in the microchannel varied from 100 to 400 nM (Fig. S1), corresponding to conditions representative of dissolved free amino acids in the ocean (15), and resulting in a steady linear gradient of 0.5 nM/μm. We identified and tracked individual cells via video microscopy and determined the chemotactic response of the population by quantifying the steady-state chemotactic distribution of cells along the serine gradient (Fig. 1). This revealed a strong accumulation of cells in the direction of increasing serine concentration, with 60% of the cells accumulated in the 100-μm region at the top of the 600-μm-wide gradient (Fig. 1*C*, black).

Single-cell tracking allowed us to quantify the natural variation of swimming speed within the population (Fig. 1*A*) and revealed that the distribution of speeds is well approximated by a gamma function (shape parameter, 8.8; scale parameter, 4.3). The average swimming speed V of each cell was computed by averaging its instantaneous speed over the duration of its trajectory. This approach is justified because the magnitudes of swimming speed fluctuations in a trajectory relative to the mean are moderate (on average, 39 ± 6%). We could thus bin cells in the analysis based on their swimming speed and therefore separately consider the chemotactic distribution of cells having different speeds (Fig. 1 *A* and *B*). We further increased the dynamic range of the swimming speed by using a range of sodium concentrations in the solution, $[Na^+]$ = 3–600 mM, exploiting the fact that the motor of *V. alginolyticus* is driven by transmembrane sodium gradients (10), so that the cells' swimming speed (averaged over the population) increases

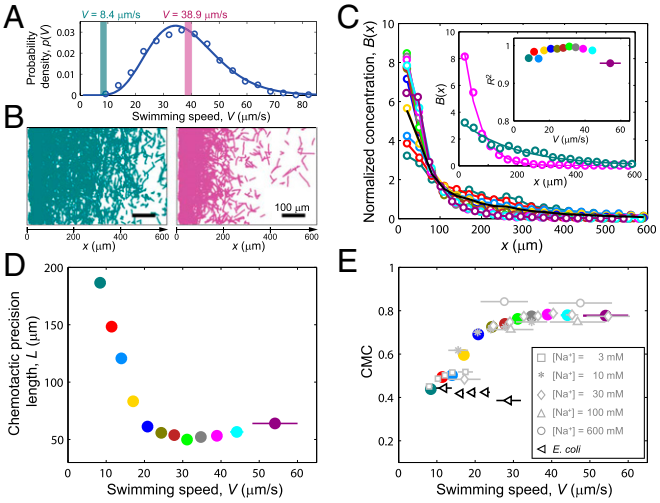

Fig. 1. The chemotactic precision of *V. alginolyticus* increases with swimming speed. (*A*) Distribution of swimming speeds, $p(V)$, within a *V. alginolyticus* population in the presence of a serine gradient (defined in Fig. S1). The swimming-speed distribution (markers) is well fitted by a gamma distribution (line). The shaded boxes denote two speed bins: V = 8.4 ± 1.2 μm/s (teal) and V = 38.9 ± 1.3 μm/s (magenta) (*B* and *C*). (*B*) Single-cell trajectories at steady-state accumulation for cells belonging to the two speed bins identified in *A*. Note the considerably tighter accumulation of the faster cells (magenta) in the region of high serine concentration (toward x = 0). (*C*) Steady-state bacterial concentration profiles, $B(x)$, for cells belonging to different speed bins (see *Inset* for speed color coding) in the same serine gradient as in *B*. Data were collected over a range of sodium concentrations (3–600 mM) and trajectories were binned into 12 speed bins based on the average swimming speed, V. Each of the 12 speed bins is 2.5–6.1 μm/s wide, except for the highest speed bin (40.5 μm/s wide), and contains the same number of trajectories (4,643). The bacterial distribution $B(x)$ for each speed bin was normalized to a mean of 1. The black line denotes the overall bacterial concentration profile before speed binning. (*C*, *Inset*) Bacterial distributions are well fitted by an exponential function, as illustrated for $B(x)$ pertaining to the two speed bins shown in *B*. (*C*, second *Inset*) The exponential fit is good for all speed bins, as demonstrated by R^2 values consistently close to 1. (*D*) Chemotactic precision length scale, L, obtained as the decay length scale of the exponential fits to $B(x)$ for each of the 12 speed bins shown in *C*. A low value of L corresponds to a tight accumulation, hence to high chemotactic precision. (*E*) Chemotactic migration coefficient, CMC, for each of the 12 speed bins shown in *C*. A high value of the CMC corresponds to a tight accumulation, hence to high chemotactic precision. Gray symbols represent the same data, where speed binning was performed separately for each sodium concentration, $[Na^+]$. The CMC values for *E. coli* responding to a gradient of α-methylaspartate (from 20 to 80 μM) in the same microfluidic device (Fig. S1) are shown for comparison, divided into five speed bins (black open triangles). For *C*–*E*, horizontal error bars denote SDs of each speed bin. Where not visible, horizontal error bars are smaller than symbols.

with the sodium concentration, according to $V = V_0\,[Na^+]/(14.9 + [Na^+])$, where V_0 = 47.5 μm/s (10). Overall, we quantified the chemotaxis of 55,718 individual cells: in the analysis, each cell was assigned to 1 of 12 speed bins, ranging from 8.4 ± 1.2 to 54.1 ± 5.9 μm/s, based on its swimming speed. In the following, we refer to this process as speed-based binning and to different ranges of speed as speed bins, for brevity. Different speed bins had different widths so that each bin contained the same number of cell trajectories, for statistical robustness in the computation of swimming kinematics.

This speed-based binning revealed a stark difference in the steady-state chemotactic accumulation of cells swimming at different speeds (Fig. 1*B*). Faster cells accumulated more tightly than slower cells, as seen by comparing a slow-speed bin, V = 8.4 ± 1.2 μm/s, and a fast-speed bin, V = 38.9 ± 1.3 μm/s (Fig. 1*B*). To quantitatively determine the dependence of the strength of accumulation on the swimming speed, we computed the bacterial

distribution along the chemoattractant gradient, $B(x)$, separately for each speed bin (Fig. 1*C*). The distributions $B(x)$ corresponding to the 12 speed bins clearly demonstrate that faster cells have higher chemotactic precision, accumulating more tightly in the high-serine region than slower cells.

Two metrics were used to quantify the speed dependence of chemotaxis in *V. alginolyticus*. First, the cell distribution profile $B(x)$ for each speed bin was fitted by an exponential, $B(x) = B_0 \exp(-x/L)$, where x is the direction along the chemoattractant gradient, L is the exponential decay length, and B_0 is a normalization constant (Fig. 1*C* and *Inset*). The exponential distribution is the steady-state solution of classic formulations of the bacterial transport equation (13) (Keller–Segel's formulation). We found that an exponential distribution is a very good fit for all 12 speed bins ($R^2 > 0.95$; Fig. 1*C*, inner *Inset*). Thus, the exponential decay length scale, L, provides a robust metric for the chemotactic precision: the smaller L, the tighter the accumulation. For *V. alginolyticus*, L decreased from 187 μm at $V = 8.4 \pm 1.2$ μm/s to 54 μm at $V = 27.8 \pm 0.95$ μm/s, indicating a tighter accumulation with increasing speed in this range, and remained nearly constant for higher speeds (Fig. 1*D*). For comparison, the full population (Fig. 1*C*, black) had $L = 88$ μm.

As a second metric of the speed dependence of chemotaxis, we computed the chemotactic migration coefficient (16), $\mathrm{CMC} = (\langle x \rangle - W/2)/(W/2)$, a widely used parameter in the chemotaxis literature (16) that measures the displacement of a population's center of mass, $\langle x \rangle = \int xB(x)dx$, from the central point in the gradient ($x = W/2$), with $W = 600$ μm being the spatial extent of the gradient (here, the microchannel's width). CMC = 0 signifies no chemotactic response, CMC = 1 is maximum attraction, and CMC = −1 is maximum repulsion. We found that the CMC increased from 0.44 at $V = 8.4 \pm 1.2$ μm/s to 0.74 at $V = 27.8 \pm 0.95$ μm/s, and saturated for higher speeds (Fig. 1*E*), confirming the trend revealed by the chemotactic precision length scale, L (Fig. 1*D*) (for the full population, the CMC was 0.59). We could rule out the possibility that the change in accumulation strength with speed was due to physiological changes arising from different sodium concentrations, as the same speed dependence of the CMC was obtained when cells were binned by speed separately for each sodium concentration (Fig. 1*E*, gray symbols). Based on these results, in the subsequent analysis we consider a low-speed regime comprising speed bins below $V = 30$ μm/s and having lower chemotactic performance, and a high-speed regime comprising speed bins above $V = 30$ μm/s and having higher chemotactic performance.

Whereas it is intuitive that chemotactic cells obtain a benefit from swimming faster—because they can climb resource gradients more rapidly (Fig. S3)—the tighter steady-state accumulation of faster cells at the peak of a resource gradient is unexpected and represents an additional benefit of enhanced speed. This speed dependence is absent in *E. coli*, as we confirmed by repeating experiments with this bacterium exposed to a gradient of 20–80 μM α-methylaspartate (Fig. 1*E*, black symbols), a commonly used chemoattractant for *E. coli*, in a range of concentrations known to elicit strong chemotaxis (17). Although *E. coli* displayed a smaller dynamic range of swimming speeds ($V = 11.9 \pm 2.1$ to 28.8 ± 3.2 μm/s), this range was sufficiently wide to consider five speed bins and establish that the chemotactic precision was independent of swimming speed (CMC = 0.42 ± 0.02). Furthermore, the fact that the maximum CMC of *E. coli* responding to optimal concentrations of one of its strongest attractants was on the lower end of the CMC of *V. alginolyticus* responding to nanomolar serine concentrations underscores the strong chemotactic capabilities of marine bacteria reported in literature (5, 6).

Strong Chemotaxis at High Swimming Speeds Results from Reduced Randomness. To understand the origin of the observed speed dependence of chemotaxis, we first quantified population-level swimming statistics—the random motility D and the chemotactic velocity V_C—as a function of swimming speed. The chemotactic velocity measures the net speed at which cells move up the gradient, and the translational diffusivity (also called "random motility") measures the intrinsic randomness of the swimming pattern and limits the level of accumulation a population can achieve. The precision with which a population of microorganisms accumulates at the peak of a resource gradient is determined by the competition between these two properties, with higher V_C enhancing chemotactic precision and higher D reducing it. As predicted by an advection–diffusion model of bacterial transport (13), in a linear chemoattractant gradient the steady-state bacterial distribution is exponential, $B(x) = B_0 \exp(-x/L)$, with the length scale $L = D/V_C$ (thus, our exponential fit to observed distribution profiles in Fig. 1*C*). To gain insights into the observed speed dependence of the chemotactic precision length scale L (Fig. 1*D*), we thus separately consider how D and V_C vary with speed (Fig. 2).

We computed the random component of motility, D, for each speed bin based on a theoretical formulation recently derived for run–reverse–flick motility (18), yielding $D = (V^2/6)[(f + 4D_R)/(f + 2D_R)^2]$. The reorientation frequency f was quantified from individual bacterial trajectories (Fig. 3) and the rotational diffusivity D_R (measuring the gradual change in orientation during runs due to Brownian rotation and off-axis propulsion) was obtained from a resistive force model (11) (*SI Materials and Methods*). Two features stand out from the computed values of the random motility. First, D increases quadratically with speed, $D \sim V^2$, in the high-speed regime ($V > 30$ μm/s), but linearly in the low-speed regime, where $D \sim V$ (Fig. 2*A*, *Inset*, and Table S1). Thus, at high swimming speeds, the effect of random motility in hindering tight accumulation is not as strong. This feature, as will be seen below, is at the heart of the high chemotactic precision of fast *V. alginolyticus* cells.

Second, run–reverse–flick swimming is characterized by a low value of the random component of motility. This can be seen by comparing D for *V. alginolyticus* and *E. coli*, where the latter was calculated as $D = V^2/(3f(1 - \alpha))$ (2), with $f = 1$/s being *E. coli*'s tumbling frequency and $\alpha = 0.33$ being persistence, defined as the mean of the cosine of the reorientation angle between runs. When the comparison is performed at natural swimming speeds [47.5 μm/s for *V. alginolyticus* (10); 19.7 μm/s for *E. coli* (Fig. 1*E*) (2)], the random motility of *V. alginolyticus* ($D = 160.8$ μm^2/s for the speed bin $V = 47.5 \pm 1.4$ μm/s) was 17% smaller than that of *E. coli* ($D = 193.1$ μm^2/s), despite the 2.4-fold higher speed. When the comparison is performed at *E. coli*'s natural swimming speed (using the speed bin $V = 19.2 \pm 2.2$ μm/s for *V. alginolyticus*), the random motility of *V. alginolyticus* ($D = 44.5$ μm^2/s; Fig. 2*A*) was 77% smaller than that of *E. coli* ($D = 193.1$ μm^2/s). This comparison confirms the prediction of a recent model (19) that run–reverse–flick motility—owing to the presence of reversals—has lower randomness than run-and-tumble motility, and the reduction in the value of D determined here (77%) is quantitatively even

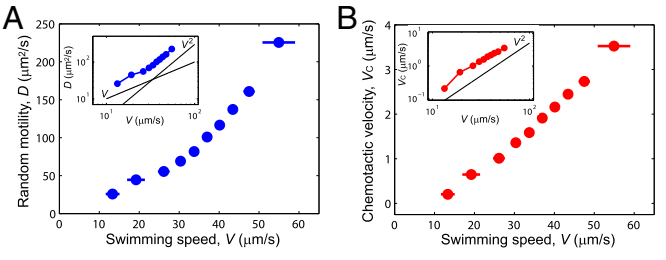

Fig. 2. The random and directional components of swimming in *V. alginolyticus* in a serine gradient (Fig. S1). (*A*) The random motility coefficient, D, and (*B*) the chemotactic velocity, V_C, as a function of swimming speed, V. Data were collected over a range of sodium concentrations (3–600 mM) and binned by speed. *Insets* show the same data in log-log format, with black lines denoting the V and V^2 slopes for reference (Table S1). For both panels, horizontal error bars denote SDs of each speed bin.

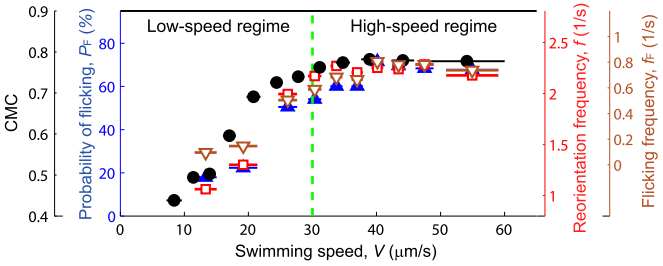

Fig. 3. The swimming kinematics of *V. alginolyticus* reveal a low-speed ($V <$ 30 μm/s) and a high-speed ($V >$ 30 μm/s) regime. CMC (black circles), probability of flicking, P_F (blue upright triangles), reorientation frequency, f (red squares), and flicking frequency, f_F (brown inverted triangle), as a function of speed V in a serine gradient (as in Fig. S1). The green dashed line marks the threshold, V = 30 μm/s, between the low-speed and the high-speed regimes. Horizontal error bars denote SDs of each speed bin.

larger than that predicted theoretically (19) (50%). This reduced diffusivity contributes to explain the much higher chemotactic precision of *V. alginolyticus* compared with *E. coli*, both at natural swimming speeds (CMC = 0.79 for *V. alginolyticus* swimming at 47.5 μm/s; CMC = 0.42 for *E. coli* swimming at 19.7 μm/s) and for the same swimming speed (CMC = 0.66 for *V. alginolyticus* swimming at 19.7 μm/s, obtained by interpolation of the CMC values as a function of swimming speed) (Fig. 1*E*).

The chemotactic velocity, V_C, was computed as $V_C = D/L$ using the value of the length scale L determined from the exponential fit to the population accumulation profile (13) (Fig. 1*D*). This revealed a quadratic dependence of V_C on the swimming speed, $V_C \sim V^2$, over the entire range of swimming speeds (Fig. 2*B*, *Inset* and Table S1). This result is in line with predictions from recent theoretical models for *E. coli* and *V. alginolyticus* (18, 20) and, to the best of our knowledge, represents the first experimental quantification of the dependence of the chemotactic velocity on the swimming speed. The steady-state chemotactic velocities ranged from V_C = 0.2–3.5 μm/s (Fig. 2*B*), corresponding to a relative chemotactic velocity V_C/V of <10%. The ratio V_C/V is a measure of the directionality of the response: less than 10% of the swimming speed of *V. alginolyticus* is on average directed up the gradient at steady state. This level of directionality is on par with that of *E. coli*, which often is in the range of 5–10% (21). Although the relative chemotactic velocity can be higher for particular gradients and types of chemoattractants [up to 35% (21)], our observations indicate that *V. alginolyticus*' higher performance in accumulating at resource peaks was not due to a higher chemotactic velocity but rather to a lower random motility (Fig. 2*A*). This conclusion is also in line with a recent theoretical model, which predicts that run–reverse–flick swimmers have lower diffusivity but the same chemotactic velocity as run-and-tumble swimmers, for the same swimming speed (19).

Reduced Randomness at High Speeds Is Caused by an Enhanced Reorientation Frequency. To understand the changeover between a quadratic and a linear dependence of random motility on swimming speed, which is at the origin of the speed-dependent chemotactic precision of marine bacteria, we quantified single-cell–level swimming kinematics—the reorientation frequency f and the probability of flicking P_F—as a function of swimming speed (Fig. 3). The reorientation frequency, f, was computed by identifying both the reversals and the flicks from trajectories (*SI Materials and Methods*). A modulation of the reorientation frequency is typically at the origin of the cells' response to chemical gradients (2, 4). Here, however, we also quantified f in the absence of gradients to focus on its dependence on swimming speed, V (Fig. S4). We found that f increased linearly with V in the low-speed regime ($V <$ 30 μm/s) and was independent of V in the high-speed regime ($V >$ 30 μm/s) (Fig. S4*B*), and that the same trend occurred in the presence of a serine gradient (Fig. S4*A*), signifying that *V. alginolyticus* modulates its reorientation frequency as a function of swimming speed.

This result explains the observed speed dependence of the random motility. This can be seen by considering the theoretically predicted random motility for run–reverse–flick swimming, $D = (V^2/6)\,[(f + 4D_R)/(f + 2D_R)^2]$ (ref. 18; described above), which in the limit of negligible rotational diffusion ($D_R << f$) becomes $D = (V^2/6f)$. This relation predicts $D \sim V$ in the low-speed regime, where $f \sim V$, and $D \sim V^2$ in the high-speed regime, where f is independent of V: both predictions successfully describe the observed dependence of D on V (Fig. 2*A*, *Inset*, and Table S1).

Not only the frequency of all reorientations, f, depended on swimming speed, but also and even more so the frequency of flicks, f_F, which displayed an approximately eightfold increase from f_F = 0.095 flicks per s at V = 13.3 ± 1.7 μm/s to f_F = 0.78 flicks per s at V = 47.5 ± 1.4 μm/s (Fig. 3, brown). The frequency of flicks is given by $f_F = f/2 \times P_F$, where P_F is the probability of flicking (the probability that the onset of a forward run is immediately followed by a flick; *SI Materials and Methods*). The factor of 2 arises because flicks can occur at most every other reorientation (i.e., only after the start of a forward run) (10). The eightfold increase in f_F with speed was due in part to a twofold increase (from 1.1/s to 2.3/s) in the overall reorientation frequency, f, and mostly to a fourfold increase in P_F (from 18% to 68%) (Fig. 3). The increase of P_F with V is in line with previous results in the absence of chemical gradients (10) and was here also observed in the presence of a gradient (Fig. 3, blue). The functional dependence of both P_F and f_F on V mirrors that of the reorientation frequency, f, and the chemotactic migration coefficient, CMC (Fig. 3, black), further highlighting the connection between the rate and nature of reorientations and the chemotactic precision.

Our data suggest that the dependence of reorientation frequency f, probability of flicking P_F, and consequently flicking frequency f_F on the swimming speed V is largely independent of gradient sensing. For P_F, this conclusion is supported by the biomechanics of flicking, which results from a buckling instability that is independent of chemical gradients, as well as by a comparison of the dependence of P_F on V in the presence (Fig. 3) and absence (10) of a serine gradient. For f, the conclusion is also supported by comparing observations in the presence (Fig. S4*A*) and absence (Fig. S4*B*) of a serine gradient: even in homogeneous conditions, f depends strongly on V (Fig. S4*B*), and, small differences in absolute values notwithstanding, this dependency is similar with and without a gradient. Binning the data by sodium concentration allowed us to exclude the potential for this observation to originate from physiological effects of different sodium concentrations (10) (Fig. S4; gray symbols). This observation supports the conclusion that swimming speed itself is an important determinant of the probability of flicking and the reorientation frequency, irrespective of the presence or absence of a chemical gradient. Because the modulation of the reorientation frequency (in *E. coli*, the "tumbling rate") is the basis of bacterial chemotaxis (2, 4), this finding suggests that swimming speed plays a key role in the chemotaxis of *V. alginolyticus* and possibly of other marine bacteria, extending the current paradigm of chemotaxis based on chemical information alone.

Chemokinesis Shifts the Swimming Speed of a Population into the High-Speed Regime. The motility repertoire of *V. alginolyticus* includes a further, important adaptation—chemokinesis—that is intimately intertwined with the observed speed dependence of swimming kinematics (Fig. 3) and chemotactic precision (Fig. 1 *C* and *E*). The quantification of the distribution of speeds within a population of *V. alginolyticus* from single-cell trajectories revealed strong and rapid chemokinesis, in the form of an overall shift toward higher speeds (Fig. 4, Figs. S5 and S6, and *SI Text*).

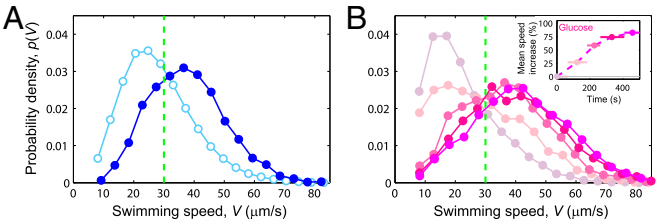

Fig. 4. Chemokinesis shifts the population's swimming speed toward the high-speed regime. (*A*) Distribution of swimming speeds, $p(V)$, within a *V. alginolyticus* population in the absence (cyan) and presence (blue) of a serine gradient (as in Fig. S1). (*B*) Temporal evolution of the swimming-speed distribution after the uniform addition of 5 μM glucose (*SI Materials and Methods*). Different shades of purple and magenta correspond to different times after glucose addition (see *Inset* for time color coding). (*B*, *Inset*) Population-averaged increase in swimming speed following 5 μM glucose addition, expressed as a percentage of the speed at time 0. Horizontal error bars denote the width of each time window. For both *A* and *B*, the green dashed line marks the speed threshold $V = 30$ μm/s, experiments were performed at a sodium concentration of 600 mM (typical of natural ocean conditions), and each curve is based on at least 2,300 trajectories.

Beyond the obvious effect of chemokinesis in enhancing chemotactic speed by accelerating gradient climbing (11), we hypothesized that chemokinesis in *V. alginolyticus* can significantly impact chemotaxis because a change in swimming speed affects all of the swimming kinematics, including the reorientation frequency and the probability of flicking (Fig. 3), and thus the cells' random motility (Fig. 2*A*). Indeed, the observed chemokinetic speed increases are sufficient to push a sizeable fraction of the population from the low-speed regime ($V < 30$ μm/s) into the high-speed regime ($V > 30$ μm/s) (Figs. 3 and 4, green dashed lines). For example, the addition of 0.5 μM serine increased the fraction of cells in the population swimming at $V > 30$ μm/s from 39% to 70% (Fig. 4*A*). Chemokinesis is thus implicated in the strong chemotactic response of *V. alginolyticus*, because faster swimming results in higher chemotactic precision.

Speed-Dependent Chemotaxis Considerably Enhances Resource Exposure. To understand how the different motility adaptations of *V. alginolyticus* affect its chemotactic performance, we developed a mathematical model of chemotaxis that, in contrast to *E. coli*'s (Fig. 5*A*), explicitly accounts for swimming speed, V, in the chemotaxis pathway (Fig. 5*B*). The model is agent-based (*Materials and Methods*) and considers variable reorientation frequency ("block R"), chemokinesis ("block C"), and flicking ("block F"), each of which depends on V (Fig. 5*B*). The model successfully captured the observed chemotactic precision in a linear chemoattractant field (Figs. S7*A* and S8*B*). We then applied it to Gaussian-shaped chemoattractant fields (Fig. S8 *C* and *D*) that mimic those occurring in the dissolved organic matter field in the ocean in the wake of sinking marine snow particles or around phytoplankton cells. We determined the relative contribution of each motility adaptation to the population-level resource exposure, by running the model for "in silico knockout mutants" (each lacking one of the chemotaxis adaptations) and comparing with the in silico wild-type cells having full chemotactic functionality (Fig. 5*C* and Fig. S8 and *SI Text*).

The absence of individual adaptations resulted in both a slower migration up the gradient (Fig. S8*A*) and a lower precision at steady state (Fig. 5*C* and Fig. S8 *B–D*). For the linear gradient used in the experiments, inhibiting chemokinesis (ΔC), flicking (ΔF), or reorientation frequency modulation (ΔR) led to 5.9–38.4% decrease in the resource exposure compared with in silico wild-type cells (Fig. 5*C*). The percent reduction for the ΔC knockout (5.9%) was comparable to the experimental value (6.8%; *SI Text*). The impact of speed-dependent chemotaxis increases considerably in more realistic, Gaussian-shaped resource landscapes. For a 1D Gaussian field, the three mutants had a 31.7–37.2% decrease in resource exposure compared with wild-type cells (Fig. 5*C*). For a 2D Gaussian field, the decrease was even larger: 35.0–58.0% when chemokinesis was caused by serine and 64.8–69.1% when it was caused by glucose (Fig. 5*C*). Comparison of the 1D and 2D scenarios suggests that the difference will be even larger in a 3D patch—for example, a phytoplankton phycosphere (22). Overall, these results show that the enhanced chemotactic precision can make a substantial difference in the ability of cells to exploit resource hot spots.

Discussion

Our results show that, contrary to what happens in the enteric bacterium *E. coli*, swimming speed and its modulation are important determinants of the chemotactic response in the marine bacterium *V. alginolyticus*. We identified two chemotactic regimes based on speed. At low speeds ($V < 30$ μm/s), the bacteria's diffusivity D scaled linearly with V and their chemotactic velocity V_C scaled quadratically with V, so that the chemotactic precision length scale $L = D/V_C \sim 1/V$ decreased with increasing speed (Fig. 1*D* and Table S1). In this regime, cells displayed constant run lengths due to the increase in the reorientation frequency with speed (Fig. 3, red) and their chemotactic precision increased with speed, as measured by the increase in CMC with V (Fig. 1*E*). In contrast, at high speeds ($V > 30$ μm/s), both D and V_C scaled quadratically with V, so that $L = D/V_C$ remained constant with speed (Fig. 1*D* and Table S1). In this high–chemotactic-performance regime, run lengths increased with speed, whereas the reorientation frequency was speed independent (Fig. 3, red) (2), and the cells' chemotactic precision saturated, as indicated by the constancy of the CMC with V (Fig. 1*E*). In summary, fast cells have in principle a large random motility ($D \sim V^2$) and should thus disperse more around a chemoattractant peak. However, fast *V. alginolyticus* cells offset this increase in random motility by increasing their reorientation frequency ($D \sim 1/f$), and thereby effectively reduce the dispersion and increasing their chemotactic precision.

Intriguingly, the distribution of swimming speeds in a *V. alginolyticus* population under natural sodium conditions and in the absence of chemoattractant gradients sits astride of the $V = 30$ μm/s speed threshold separating the low- from the high-speed regimes (Fig. 4*A*, cyan). This observation suggests that the speed distribution and its modulation in the presence of chemical gradients result from a trade-off between the nutrient uptake benefits from chemotaxis and the energetic cost of locomotion, a cost–benefit framework previously suggested for chemotaxis in turbulent flows (23). Because uptake will increase with residence time in resource-rich regions, by

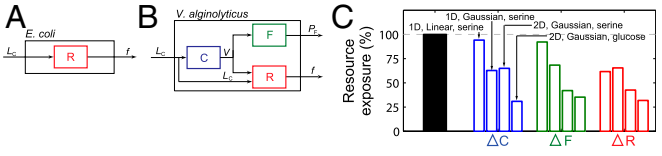

Fig. 5. A model of speed-dependent chemotaxis predicts a considerable increase in resource exposure. (*A* and *B*) System view of chemotaxis shown as block diagrams for (*A*) *E. coli* and (*B*) *V. alginolyticus*. In *E. coli*'s classic pathway, the reorientation frequency f—whose modulation enables gradient climbing—is determined solely by the sensed ligand concentration L_C (block R). In contrast, our observations suggest the presence of additional feedbacks in *V. alginolyticus*, including the ligand-dependent modulation of the speed V (chemokinesis; block C), the speed-dependent load on the flagellar hook that governs the probability of flicking P_F (block F), and the speed-dependent modulation of the reorientation frequency (block R). All of these elements involve the swimming speed V. (*C*) Population-averaged resource exposure of in silico mutants (color-coded as in *B*), expressed as a percentage of the resource exposure of in silico wild-type cells (black bar). For each case, four scenarios were evaluated, as described by labels over the bars.

being able to localize with greater precision at the resource peak, fast cells will have a fitness benefit over slow cells. At the same time, the energetic cost of swimming increases quadratically with the swimming speed (23), making fast swimming very costly relative to the potential benefits of chemotaxis in the often resource-poor marine environment (23). In this context, the cells' active ability to increase speed in favorable resource conditions—i.e., chemokinesis (Fig. 4)—represents a desirable strategy to explore the environment with reduced motility cost in the absence of nutrients, while activating the speed enhancement that yields the strongest chemotactic performance when a favorable chemical environment is sensed.

Our observation supports this cost–benefit hypothesis, for two reasons. First, the observed chemokinetic speed enhancement shifts a considerable fraction of the population from below to above the speed threshold (Fig. 4), resulting not only in a faster transient response to gradients (11) but also in a tighter steady-state accumulation of cells at the resource peak (Fig. 1 *C*–*E*). Second, the observed speed modulation is rapid, with one-half of the chemokinetic speed enhancement of a population occurring over 2–4 min (Fig. 4*B* and Fig. S5). Although some nutrient hot spots in the ocean are briefer than this, many last in the order of 10 min or more (5, 22, 23), indicating that chemokinesis can be advantageous also at the single resource patch.

Our data on the speed dependence of the swimming kinematics raise the question of whether and how bacteria sense their swimming speed (*SI Text*). Irrespectively of the origin of speed sensing, we propose that *V. alginolyticus* integrates information on its speed in its chemotaxis pathway as an additional system input to regulate reorientation frequency (Fig. 5*B*). The success of our model in capturing the experimental observations (Fig. S7*A*) lends support to the hypothesis that speed is both a system input and output of the chemotaxis pathway (Fig. 5*B*), and highlights the need to better understand, at the molecular level, both gradient sensing and speed sensing in *Vibrios*.

The results presented here reshape our understanding of bacterial motility in the ocean by demonstrating the role of swimming speed, its effect on reorientation frequency, and its modulation through chemokinesis, in determining the precision and speed of chemotaxis. The role of these motility adaptations on the ability of bacteria to exploit gradients has received only limited attention, largely owing to their absence in *E. coli*. The frequent occurrence of these chemotaxis elements among marine bacteria then suggests that speed-dependent chemotaxis may not be limited to *V. alginolyticus* but might be prevalent among sea microbes (11). Together with the large advantage in resource exposure afforded by the increase in chemotactic precision (Fig. 5*C*), this evidence suggests that this augmented form of chemotaxis, in which cellular decision-making is based on both chemical information as well as the cell's own speed, might be pervasive among marine bacteria.

We surmise that the observed speed dependence of gradient utilization among marine bacteria is related to the defining features of the marine resource landscape at the microscale, which is characterized by small, often ephemeral patches, pulses, and gradients of chemicals (8), as well as ubiquitous fluid flow that both stirs chemical resources (23) and influences bacterial motility (8). A quantitative link between the specific behavioral adaptations reported here and the features of the marine resource landscape remains to be established, and points more in general at the need for the development of an optimal foraging theory for bacteria. The observation that marine bacteria use a form of chemotaxis that is speed dependent demonstrates a previously unidentified, potentially widespread element of bacterial chemotaxis, highlights the rich adaptations in the spatial behaviors of marine bacteria, and calls for a better understanding of the ecosystem consequences of these behaviors.

Materials and Methods

Hydrogel-Based Microchannel and Cell Tracking. Both the chemotaxis and the chemokinesis experiments were performed in a hydrogel-based microfluidic device (Fig. S1) (*SI Materials and Methods*). The hydrogel agarose was used at 2% (wt/vol) concentration in milliQ water to create diffusion-permeable walls between adjacent microfluidic channels (Fig. S1). Bacteria were imaged at 22 frames per second by phase contrast microscopy (Nikon Ti-E; 20×, 0.45 N.A.).

Computational Model of Chemotaxis. An agent-based model was used to integrate in a general model of chemotaxis (24) the experimentally observed, speed-dependent motility adaptations of *V. alginolyticus*. Each agent swims in a 2D landscape made of a 1D linear, 1D Gaussian, or 2D Gaussian chemoattractant field (*SI Materials and Methods*). The population-level resource exposure was computed by weighting the chemotactic response for each speed bin with the percentage of cells in that speed bin.

ACKNOWLEDGMENTS. We thank Jeffrey Guasto for discussions. This work was supported by a Samsung Scholarship (to K.S.), NIH Grant 1R01GM100473 (to R.S.), a Wellcome Trust-University of Edinburgh Institutional Strategic Support Fund (to F.M.), and Gordon and Betty Moore Microbial Initiative Investigator Award 3783 (to R.S.).

1. Son K, Brumley DR, Stocker R (2015) Live from under the lens: Exploring microbial motility with dynamic imaging and microfluidics. *Nat Rev Microbiol* 13(12):761–775.
2. Berg HC (1993) *Random Walks in Biology* (Princeton Univ Press, Princeton).
3. Lele PP, Hosu BG, Berg HC (2013) Dynamics of mechanosensing in the bacterial flagellar motor. *Proc Natl Acad Sci USA* 110(29):11839–11844.
4. Jiang L, Ouyang Q, Tu Y (2010) Quantitative modeling of *Escherichia coli* chemotactic motion in environments varying in space and time. *PLoS Comput Biol* 6(4):e1000735.
5. Stocker R, Seymour JR, Samadani A, Hunt DE, Polz MF (2008) Rapid chemotactic response enables marine bacteria to exploit ephemeral microscale nutrient patches. *Proc Natl Acad Sci USA* 105(11):4209–4214.
6. Xie L, Altindal T, Chattopadhyay S, Wu XL (2011) From the Cover: Bacterial flagellum as a propeller and as a rudder for efficient chemotaxis. *Proc Natl Acad Sci USA* 108(6):2246–2251.
7. Stocker R (2011) Reverse and flick: Hybrid locomotion in bacteria. *Proc Natl Acad Sci USA* 108(7):2635–2636.
8. Stocker R, Seymour JR (2012) Ecology and physics of bacterial chemotaxis in the ocean. *Microbiol Mol Biol Rev* 76(4):792–812.
9. Leifson E, Cosenza BJ, Murchelano R, Cleverdon RC (1964) Motile marine bacteria. I. Techniques, ecology, and general characteristics. *J Bacteriol* 87(3):652–666.
10. Son K, Guasto JS, Stocker R (2013) Bacteria can exploit a flagellar buckling instability to change direction. *Nat Phys* 9(8):494–498.
11. Garren M, et al. (2014) A bacterial pathogen uses dimethylsulfoniopropionate as a cue to target heat-stressed corals. *ISME J* 8(5):999–1007.
12. Barbara GM, Mitchell JG (2003) Bacterial tracking of motile algae. *FEMS Microbiol Ecol* 44(1):79–87.
13. Tindall MJ, Maini PK, Porter SL, Armitage JP (2008) Overview of mathematical approaches used to model bacterial chemotaxis II: Bacterial populations. *Bull Math Biol* 70(6):1570–1607.
14. Deepika D, Karmakar R, Tirumkudulu MS, Venkatesh KV (2015) Variation in swimming speed of *Escherichia coli* in response to attractant. *Arch Microbiol* 197(2):211–222.
15. Azam F, Malfatti F (2007) Microbial structuring of marine ecosystems. *Nat Rev Microbiol* 5(10):782–791.
16. Mao H, Cremer PS, Manson MD (2003) A sensitive, versatile microfluidic assay for bacterial chemotaxis. *Proc Natl Acad Sci USA* 100(9):5449–5454.
17. Lazova MD, Ahmed T, Bellomo D, Stocker R, Shimizu TS (2011) Response rescaling in bacterial chemotaxis. *Proc Natl Acad Sci USA* 108(33):13870–13875.
18. Taktikos J, Stark H, Zaburdaev V (2013) How the motility pattern of bacteria affects their dispersal and chemotaxis. *PLoS One* 8(12):e81936.
19. Xie L, Wu XL (2014) Bacterial motility patterns reveal importance of exploitation over exploration in marine microhabitats. Part I: Theory. *Biophys J* 107(7):1712–1720.
20. Locsei JT, Pedley TJ (2009) Bacterial tracking of motile algae assisted by algal cell's vorticity field. *Microb Ecol* 58(1):63–74.
21. Ahmed T, Stocker R (2008) Experimental verification of the behavioral foundation of bacterial transport parameters using microfluidics. *Biophys J* 95(9):4481–4493.
22. Smriga S, Fernandez VI, Mitchell JG, Stocker R (2016) Chemotaxis toward phytoplankton drives organic matter partitioning among marine bacteria. *Proc Natl Acad Sci USA* 113(6):1576–1581.
23. Taylor JR, Stocker R (2012) Trade-offs of chemotactic foraging in turbulent water. *Science* 338(6107):675–679.
24. Jackson GA (1987) Simulating chemosensory responses of marine microorganisms. *Limnol Oceanogr* 32(6):1253–1266.
25. Kiorboe T, Jackson GA (2001) Marine snow, organic solute plumes, and optimal chemosensory behavior of bacteria. *Limnol Oceanogr* 46(6):1309–1318.
26. Seymour JR, Marcos, Stocker R (2009) Resource patch formation and exploitation throughout the marine microbial food web. *Am Nat* 173(1):E15–E29.
27. Kawagishi I, Imagawa M, Imae Y, McCarter L, Homma M (1996) The sodium-driven polar flagellar motor of marine *Vibrio* as the mechanosensor that regulates lateral flagellar expression. *Mol Microbiol* 20(4):693–699.